

A DIFFERENTIAL METHOD FOR SOLVING THE BOUNDARY
LAYER EQUATION FOR STEADY LAMINAR INCOMPRESSIBLE
FLOW

W. Schönauer

Translation of: "Ein Differenzenverfahren
zur Lösung der Grenzschichtgleichung für
stationäre, laminare, inkompressible
Strömung," Ingenieur Archiv, Vol. 33, 1964,
pp. 173-189.

(NASA-TT-F-14363) A DIFFERENTIAL METHOD
FOR SOLVING THE BOUNDARY LAYER EQUATION FOR
STEADY LAMINAR INCOMPRESSIBLE FLOW W.
Schoenauer (Scientific Translation Service)
Jul. 1972 36 p

N72-27314

Unclass
34037

CSCL 20D G3/12

Reproduced by
NATIONAL TECHNICAL
INFORMATION SERVICE
U S Department of Commerce
Springfield VA 22151

NATIONAL AERONAUTICS AND SPACE ADMINISTRATION
WASHINGTON, D. C. 20546 JULY 1972

N O T I C E

**THIS DOCUMENT HAS BEEN REPRODUCED FROM THE
BEST COPY FURNISHED US BY THE SPONSORING
AGENCY. ALTHOUGH IT IS RECOGNIZED THAT CER-
TAIN PORTIONS ARE ILLEGIBLE, IT IS BEING RE-
LEASED IN THE INTEREST OF MAKING AVAILABLE
AS MUCH INFORMATION AS POSSIBLE.**

A DIFFERENTIAL METHOD FOR SOLVING THE BOUNDARY LAYER EQUATION FOR STEADY LAMINAR INCOMPRESSIBLE FLOW ⁽¹⁾

by
W. Schönauer

ABSTRACT: An implicit differential method is given for the laminar incompressible steady boundary layer at a solid impermeable wall. It can be shown that perturbations are definitely reduced after a few steps of calculation. The method is tested practically with a large number of examples. An electronic computer is required, but the method is well suited for programming. Two-digit precision can be attained for the shear stress at low cost.

1. INTRODUCTION

/173*

a. The Prandtl boundary layer equations.

For steady, laminar, incompressible flows, the Prandtl [1] boundary layer equations, which are a first approximation to the Navier-Stokes equations for high Reynolds numbers, [2] are:

$$u u_x + v u_y - U U' - \nu u_{yy} = 0, \quad (1a)$$

$$u_x + v_y = 0, \quad (1b)$$

where $U(x)$ is the given outside velocity and ν is the kinematic viscosity. The velocity components within the boundary layer, $u(x, y)$ and $v(x, y)$, are desired. In general, only the "velocity profile" $u(x, y)$ or the derived quantities, wall friction stress, displacement loss thickness, and momentum thickness, are of interest.

* Numbers in the margin indicate pagination in the foreign text.

(1) Extracted from the Karlsruhe Technical College Dissertation, 1963, or from Report D7 of the Institute for Applied Mathematics, Karlsruhe Technical College.

Equations (1a) and (1b) can be solved under the following boundary conditions:

1. Transition to the outside flow:

$$y = \infty: \quad u(x, \infty) = U(x) \quad (2a)$$

and as much as possible $u_y(x, \infty) = u_{yy}(x, \infty) = \dots = 0;$

2. Adhesion condition at the solid impermeable wall:

$$y = 0: \quad u(x, 0) = v(x, 0) = 0. \quad (2b)$$

3. Furthermore, let an initial profile be given:

$$x = 0: \quad u(0, y) = \tilde{u}(y). \quad (2c)$$

b. Solution methods.

For a numerical solution of (1) and (2), principally the following methods are used:

1. Series method. $U(x)$ must be stated as a power series in x . The velocity profile $u(x, y)$ is likewise developed as a power series in x with coefficients independent of y , and universally calculable on appropriate division. The accuracy of the method depends on the convergence of the series. For large values of x , particularly near a separation point, so many series terms must be considered that the application of the method is no longer practical.

2. Momentum and energy conservation methods. With a prescribed trial function for the boundary layer profile, the boundary layer equation is fulfilled on the average across the boundary layer thickness with the laws of conservation of momentum (and energy). In this way we get an approximation to the boundary

layer equation. But we have little chance of estimating the error which may have occurred. The computing cost is relatively low.

3. Differential methods. The solution $u(x, y)$ is calculated at the lattice points of a difference network. The accuracy depends on the mesh width of the network. The computing cost is very high for high accuracy. Determination of the numerical stability is a prerequisite for the reliability of the method.

4. Method of differences and differential equations. Differences are introduced in the x -direction, while differential equations, which are to be solved as boundary value problems, are retained in the y -direction. Iterations are required for this, and these require even higher computing cost than in the differential method.

c. Similar solutions

The so-called "similar solutions" make up a class of exact solutions of (1) and (2), which we will need later. With a boundary layer thickness $\delta(x)$ and a profile parameter $\lambda(x)$, we can set up an initial boundary layer profile

$$u(x, y) = U(x) f'(\eta, \lambda)$$

with $\eta = y/\delta$. It appears that for

$$\frac{U \delta^2}{\nu} = \frac{2 \int_0^\infty U(x_1) dx_1}{U(x)} = A(x) \quad (3)$$

with x_1 as an integration variable and

$$\lambda = \frac{\delta^2 U'}{\nu} = A \frac{U'}{U} \quad (4)$$

with $\lambda = \text{constant}$, that the system (1), (2) leads to a common boundary value problem, the so-called Falkner-Skan equation [3], the solutions of which are the well-known Hartree profile [4] (Figure 1).

The requirement that $\lambda = \text{constant}$, with (4), establishes the outside velocity:

$$U(x) = cx^{\frac{\lambda}{2-\lambda}}, \quad (5)$$

which can be explained as the potential velocity at a wedge upon which the flow is symmetric, with the apex angle 2α (Figure 2). For $\lambda = 1$ we have stagnation point flow, and for $\lambda = 0$, plane plate flow.

2. THE STARTING EQUATION FOR THE DIFFERENTIAL METHOD

a. The Crocco transformation.

The Prandtl equations (1) are poorly suited for a differential method, as the integration range in the y -direction is infinite. Thus, Crocco [5] transformed the (x, y) region into an (x, u) region having the range limits $u = U(x)$. Crocco took as the dependent variable the shearing stress

$$\tau(x, u) = \bar{\rho} \nu u_y, \quad (6)$$

with $\bar{\rho}$ as the density of the flow medium.

In the incompressible case, $\bar{\rho}$ is constant. Thus, we take the dependent variable

$$u(x, u) = \frac{\tau(x, u)}{\bar{\rho} \nu} = u_y. \quad (7)$$

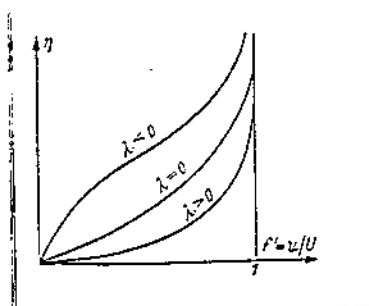


Figure 1.
Hartree profile.

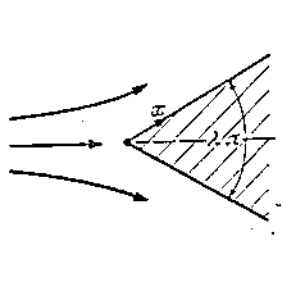


Figure 2.
The flow around
a cone.

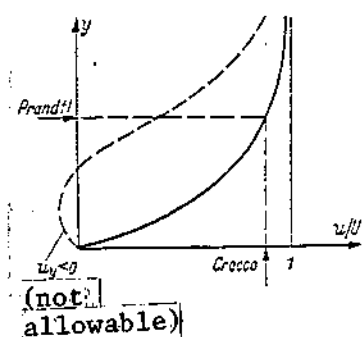


Figure 3.
Calculation of the
velocity profile
according to Prandtl
and Crocco.

Instead of the u -profile in (1) we use the t -profile. In order to obtain the velocity profile from this, we calculate the value y for u as the fixed position x (Figure 3). We have $dy = du/u_y$, and with (7)

$$y = \int_0^u \frac{du_1}{t(x, u_1)}, \quad (8)$$

where u_1 is the integration variable and x is fixed. For the back-flow profile ($t = u_y < 0$), the Crocco transformation is no longer reasonable (Figure 3).

If we transform the system (1), (2) to the t -variable with (7), then a non-linear boundary condition appears at the wall. But if we introduce the new dependent variable

$$z(x, u) = \frac{t^2}{2} \quad (9)$$

all the boundary conditions become linear, an advantage for the differential method. It appears later that the z -profiles are better handled numerically than the t -profiles, and that the z -profiles avoid the singularity which occurs with the

t-profiles near the separation point.

The system (1), (2) is transformed to the z-variable with (7) and (9). With respect to the derivation of the z-equation, see Schönauer ⁽²⁾, Section 4. From (1) we obtain

$$u z_x + U U' z_u - \nu (2 z z_{uu} - z_u^2) = 0, \quad (10)$$

and the conditions (2) become

1. Transition to outside flow

$$u = U(x) : z(x, U) = 0; \quad (11a)$$

2. Wall

$$u = 0 : z_u(x, 0) = -\frac{U U'}{\nu}; \quad (11b)$$

3. Initial profile

$$x = 0 : z(0, u) = \bar{z}(u). \quad (11c)$$

b. Similarity transformation.

As was described in Section 1c, the Prandtl equations (1) can be transformed by a similarity transformation into a form from which similar solutions can be obtained at once. Now we shall likewise make a similarity rule for the z-variable, in which $\delta(x)$ and $\lambda(x)$ are defined by equations (3) and (4). Because δ often appears in the combination $U \delta^{2/\nu} = A(x)$, this quantity is defined in (3).

In order to obtain dimensionless quantities, we introduce in place of u:

$$\zeta = \frac{u}{U} \quad (12)$$

(2) See footnote (1), page 1.

and obtain, instead of the variable range limit $u = U(x)$, the fixed limit $\xi = 1$ (rectangular range).

We make the variable x dimensionless by a fixed reference length L . Then the argument x/L is to be inserted in all functions of x . Likewise, the integration variable x_1/L is to be taken in (3), and we have

$$A(x) = L A_L(x/L). \quad (13)$$

$A(x)$ has the dimension of length and $A_L(x/L)$ is dimensionless. For λ we have

$$\lambda(x/L) = A_L U(x/L) / U'(x/L) \quad \text{with} \quad U'(x/L) = dU/d(x/L).$$

The dependent variable z has the dimension of u_y^2 , so for z we make the statement

$$z(x, u) = \frac{U^2}{\delta^2} H(\xi, x/L). \quad (14)$$

As U and δ are unknown functions, solution of the boundary layer equation is reduced to calculation of the dimensionless quantity H .

With (3), (4), (13), and (14) we get an equation for the H -profile from (10). For its derivation, see Schönauer, Section 5 (3). With the designation $H' = \partial H / \partial \xi$ we get

$$\frac{1}{A_L} [2 H H'' - H'^2 - \lambda (1 - \xi^2) H' - (4\lambda - 2) \xi H] - \xi H_{x/L} = 0. \quad (15)$$

This equation is the starting point for the differential method.

Equation (15) was given by Nickel [6]. Gadd [7] used a similar equation for the laminar compressible boundary layer.

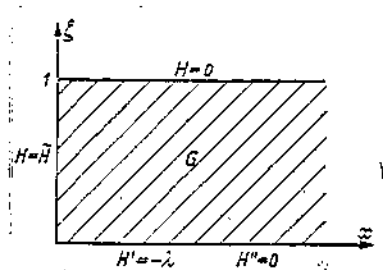
(3) See Footnote (1), page 1.

Conditions (11) yield

$$\zeta = 1 : H(1, x) = 0, \quad (16a)$$

$$\zeta = 0 : H'(0, x) = -\lambda, \quad (16b)$$

$$x = 0 : H(\zeta, 0) = \tilde{H}(\zeta). \quad (16c)$$



The so-called second wall
adhesion follows from (15)
and (16b):

Figure 4. Integration range
and boundary conditions
for Equation (15).

$$\zeta = 0 : H''(0, x) = 0. \quad (16d)$$

Figure 4 shows the integration range with the boundary conditions.

/176

In the following deliberations we shall, for simplicity, set $L = 1$ and only consider the reference length L again in Section 8.

3. THE SIMILAR SOLUTIONS OF THE H-EQUATION

If we set the large term in parentheses in (15) equal to zero, and λ is constant:

$$2H H'' - H'^2 - \lambda(1 - \zeta^2) H' - (4\lambda - 2)\zeta H = 0, \quad (17)$$

then all the coefficients of this equation and the boundary conditions (16a) and (16b), which satisfy a solution of (17), are constant. Then a profile $H = H(\zeta)$ can be found as a solution of this ordinary boundary value problem, which satisfies (17) independently of x , and so also satisfies (15). Figure 5 shows some similar H profiles. They are the

H-transformed Hartree profiles ⁽⁴⁾, which include an outside velocity according to (5).

Rauer [8] has calculated similar H-profiles with high accuracy and was able to show that the asymptotic development

$$\zeta \rightarrow 1: H(\zeta) \rightarrow (1 - \zeta^2) [a + b \ln(1 - \zeta)], \quad (18)$$

applies, where a and b are constants. Then the value $H' = 0$ for $|\zeta| = 1$. That is, the profiles open at the point $|\zeta| = 1$ with horizontal tangents. But at the same time, $H'' = \infty$. The t -profiles corresponding to the H-profiles would open at $|\zeta| = 1$ with vertical tangents (Figure 5). This singularity is more undesirable for numerical calculation than the singularity $H'' = \infty$ of the t^2 -profile. In Section 7 it is shown how the similar H-profiles can be computed iteratively by the differential method.

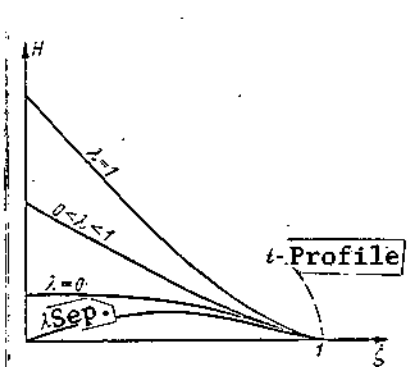


Figure 5. Similar H-profiles

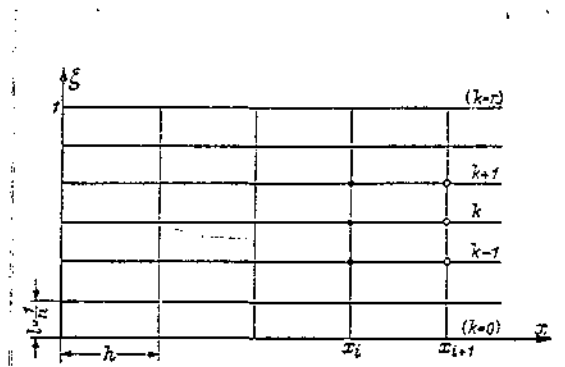


Figure 6. Symbols for the differential method

(4) See Reference 4

4. THE DIFFERENTIAL METHOD

a. Preliminary comments

Explicit differential methods ⁽⁵⁾ for the incompressible Prandtl equations were developed by Schröder [9], Görtler [10], Witting [11] and Rheinboldt [12]; for the compressible Prandtl equations by Siekmann [13]; and for the compressible Crocco equation by Flügge-Lot [14]. From the author's experience, these explicit methods are stable only at sufficiently great distance from the stagnation point and sufficiently small step width in the x-direction. Stability investigations have not been performed.

In order to obtain more favorable stability properties, Kramer and Lieberstein [15] developed an implicit differential method for the compressible Crocco equation, without demonstrating the stability, however.

While the present work was being done, implicit differential methods with stability studies were developed by Fiebig [16] for the Prandtl equations and by Krawczyk [17] for the von Mises equation.

b. Symbols for the differential method

The integration range shown in Figure 4 is covered with a rectangular lattice having the mesh width h in the x-direction and l in the η -direction (Figure 6). In the η -direction we will usually calculate with the more distinct strip number n . As the range is limited by $\eta = 1$, $l = 1/n$.

We assume that we know the solution H at a point x_i , which is also called, briefly, i , in the following.

-
- (5) A differential method is called explicit if the solution can be calculated explicitly at the lattice points, in contrast to implicit methods in which the solution is obtained by solution of a system of equations.

We will calculate the solution for position x_{i+1} according to the parabolic character of Equation (15).

As the differential method works with lattice point values, we replace the derivatives in the ξ -direction by the central difference quotients

$$H'_{i,k} = \frac{n}{2} (H_{i,k+1} - H_{i,k-1}) \left\{ -\frac{p}{6} H''' \right\}, \quad (19a)$$

$$H''_{i,k} = n^2 (H_{i,k+1} - 2H_{i,k} + H_{i,k-1}) \left\{ -\frac{p}{12} H^{IV} \right\}. \quad (19b)$$

The first neglected term of the Taylor series is always shown in (19).

We introduce the symbols

$$\Pi_i = 4 [\lambda(x_i) - 2]\xi, \quad (20a)$$

$$E_i = (1 - \xi^2) \lambda(x_i), \quad (20b)$$

$$B_i = \frac{\xi A(x_i)}{h}. \quad (20c)$$

The ordinate on a line k of the mesh network, Figure 6, is

$$\xi = \xi_k = k l = \frac{k}{n}.$$

For the large term in parentheses in (15) we use the designation

$$[i, k] = 2 H_{i,k} H'_{i,k} - H_{i,k}^2 - E_i H'_{i,k} - \Pi_i H_{i,k}.$$

c. An implicit differential method.

We replace H_x in (15) by the difference quotient

$$H_x = \frac{1}{h} (H_{i+1,k} - H_{i,k}) \left\{ -\frac{h}{2} H_{xx} \right\} \quad (21)$$

and take all H values in the brackets $[]$ of (15) at the point $i + 1$. Then, with the symbols from Section 4b, we obtain

$$[i + 1, k] - B_{i+1} (H_{i+1,k} - H_{i,k}) = 0. \quad (22)$$

Equation (22) contains three unknown H-values at the point $i + 1$ through Equations (19). Such an Equation (22) can be set up for all inner lines from $k = 1$ to $k = n - 1$. But $n + 1$ unknown H values, H_0 to H_n must be calculated. Of these, $H_n = 0$ is given from the boundary condition (16a), so that an equation for H_0 is still lacking.

In order to obtain this equation, we represent the value H_{i+1} in the ξ -direction by a Taylor expansion at the point $i + 1$. With the boundary conditions (16b) and (16d) we obtain the wall equation

$$H_{i+1,0} - H_{i+1,1} = \frac{\lambda}{n} \left\{ -\frac{\beta}{6} H''' \right\}. \quad (23)$$

The Equations (22) formed for $k = 1$ to $k = n - 1$ yield, with (23), a system of n equations for the n unknown H_0 to H_{n-1} . This system is nonlinear because of the first two terms in $[i + 1, k]$. These terms are linearized as follows:

$$\bar{H}_{i+1,k} H'_{i+1,k} = \bar{H}_{i,k} H'_{i+1,k} \{ + h H_x \}, \quad (24a)$$

$$H'^2_{i+1,k} = H'_{i,k} H'_{i+1,k} \{ + h H_x \}. \quad (24b)$$

The equation system, which is again linear, is ordered with respect to the unknowns. This yields the equations:

for $k = 0$, Equation (23) applies;
for $k = 1$ to $k = n - 1$, we have

$$c_{k,k-1} H_{i+1,k-1} + c_{k,k} H_{i+1,k} + c_{k,k+1} H_{i+1,k+1} = r_k \quad (25)$$

with the coefficients

$$c_{k,k+1} = -2n^2 H_{i,k} \pm \frac{n}{2} (H'_{i,k} + E_{i+1}) \quad (26a)$$

(with the exception that $c_{n-1, n}$ drops out);

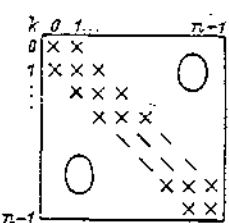
$$c_{k,k} = 4n^2 H_{i,k} + H_{i+1} + B_{i+1}, \quad (26b)$$

$$r_k = B_{i+1} H_{i,k}. \quad (26c)$$

With the vectors

$$\vec{H}_i = \begin{pmatrix} H_{i,0} \\ H_{i,1} \\ \vdots \\ H_{i,n-1} \end{pmatrix}, \quad \vec{H}_{i+1} = \begin{pmatrix} H_{i+1,0} \\ H_{i+1,1} \\ \vdots \\ H_{i+1,n-1} \end{pmatrix}, \quad \vec{r} = \begin{pmatrix} r_0 \\ r_1 \\ \vdots \\ r_{n-1} \end{pmatrix}$$

and the matrix C formed from the coefficients $c_{k, \mu}$ we can write the equation system in matrix form:

$$C(\vec{H}_i) \vec{H}_{i+1} = \vec{r}(\vec{H}_i). \quad (27)$$


Matrix C is a tridiagonal matrix (Figure 7).

Figure 7.
Tridiagonal matrix.

To solve such an equation system, we will set up a special computer subprogram, in which the null elements need not be stored. For each equation, four memory positions are required with the right side. In order to solve by the Gauss elimination method, we need three additions, three subtractions, and two divisions for each equation.

The vector \tilde{H}_{i+1} appears as the solution of system (27). In this way, the H-profile is known at point $i + 1$. Then the profile for point $i + 2$ can be computed, etc. In order to compute one value $H_{i+1, k}$, 25 arithmetic operations are required if we count only the operations to be done at each point $(i + 1, k)$ (including solution of the equation system) and assume all other quantities to be previously calculated, such as $n/2, n^2, \tilde{z}_k, (1 - \tilde{z}_k^2)$.

d. The initial profile \tilde{H} .

A profile $\tilde{H}(\xi)$ must be given as the beginning condition (16c). Essentially, any arbitrary \tilde{H} -profile can be used in this method. But it will be very suitable if the initial profile also meets the boundary conditions (16a), (16b) and (16d). For a flow body with the leading edge angle $\alpha = \lambda\pi$ (Figure 2) we will take the similar solution described in Section 3 for $\lambda = \alpha/\pi$ as the \tilde{H} -profile for point $x = 0$, for which the calculation is shown in Section 7. We can also start the calculation with $x_0 \neq 0$, and must then prescribe the profile \tilde{H} for this point.

If the profile \tilde{H} does not meet the boundary conditions (18a), (18b) and (18d), then the "compatibility condition" between the initial and the boundary conditions is not met. The solution of such a problem has a singularity at the starting point, x_0 , which in the differential method is "blurred" over a mesh width, but which does not perturb the application of the differential method.

5. THE STABILITY BEHAVIOR

The stability behavior of the differential method given above was studied directly with respect to the behavior of a small error, without being based on a stability definition. Here only the basic concept and the result of the investigation are reported.

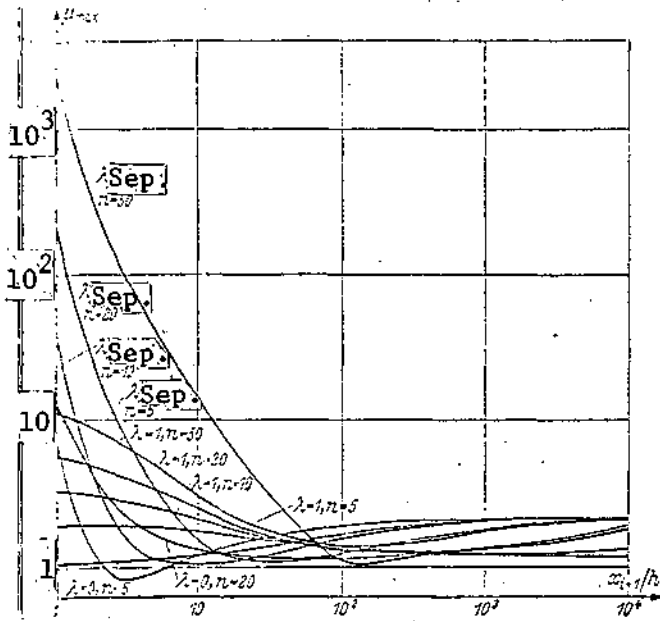


Figure 8. Eigenvalues μ_{\max} for the S'S matrices

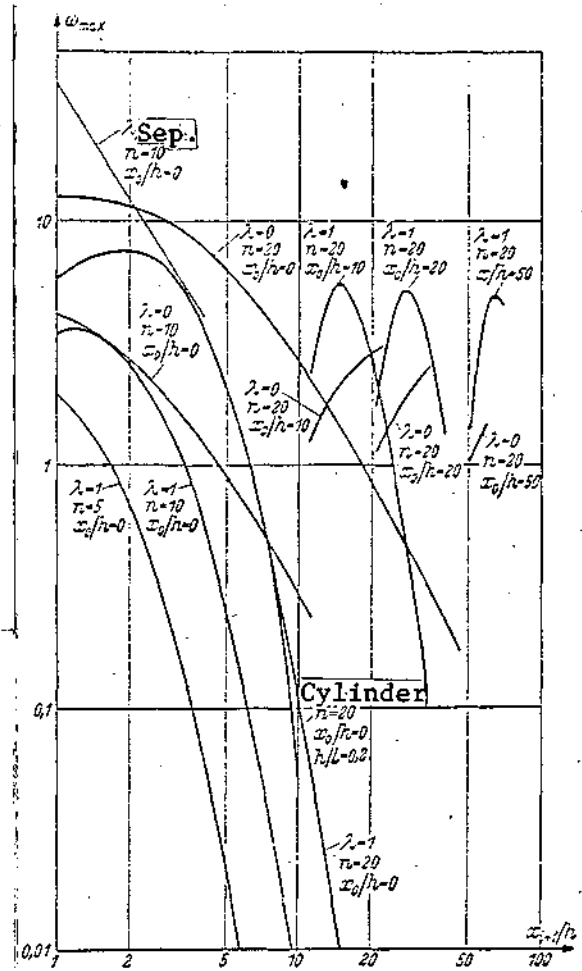
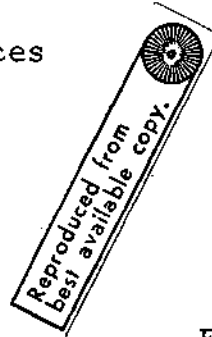


Figure 9. Eigenvalues ω_{\max} for the matrices R'R.

A starting profile \bar{H}_i at point x_i would produce an adjacent profile \bar{H}_{i+1} at point x_{i+1} as a solution of (27). An initial profile $\bar{H}_i + \bar{\varphi}_i$, where $\bar{\varphi}_i$ is an error vector assumed to be small, $\|\varphi_i\| \ll \|\bar{H}_i\|$ produces an adjacent profile $\bar{H}_{i+1} + \bar{\varphi}_{i+1}$. Linearized, then (vector arrows are now left off) we have

$$\varphi_{i+1} = S \varphi_i, \quad (28)$$

where S is a matrix which depends on the solution H_{i+1} but

is independent of $|\varphi|$. We shall call it the stability matrix.

If we consider an error φ_0 introduced at an arbitrary point x_0 over several computation steps, we get the error series: $\varphi_0; \varphi_1 = S_1 \varphi_0; \varphi_2 = S_2 \varphi_1 = S_2 S_1 \varphi_0; \dots$ etc., and generally, after m steps,

$$\varphi_m = S_m \varphi_{m-1} = S_m S_{m-1} \dots S_2 S_1 \varphi_0 = R_m \varphi_0. \quad (29)$$

We ask ourselves: how does the length of the error vector change here? If we investigate the first part of (29), that is, $\varphi_m = S_m \varphi_{m-1}$, this equation represents the behavior of the error in a (general) computational step. The length of this vector is

$$|\varphi_m|^2 = \varphi_m' \varphi_m = \varphi_{m-1}' S_m' S_m \varphi_{m-1}, \quad (30)$$

where ' designates transposition (exchange of rows and columns). With the eigenvalues $|\mu_j| \geq 0$ of the so-called Gauss-transform $S_m' S_m$ and the components a_j of the suitably transformed vector φ_{m-1} we get

$$|\varphi_{m-1}|^2 = a_1^2 + a_2^2 + \dots + a_n^2 \quad (31a)$$

and for comparison

$$|\varphi_m|^2 = \mu_1 a_1^2 + \mu_2 a_2^2 + \dots + \mu_n a_n^2 \quad (31b)$$

If all $|\mu_j| < 1$; that is, if $|\mu_{\max}| < 1$, then also $|\varphi_m| < |\varphi_{m-1}|$ and the error vector has become smaller. An increase in the error can occur with $|\mu_{\max}| > 1$.

180

The matrix $S_m' S_m$ depends on x/h , n , and the H-profile itself. The eigenvalues μ_{\max} were determined numerically for a large number of matrices $S_m' S_m$ for the H-profiles of the similar solutions. The results are shown in Figure 8. As all values of $|\mu_{\max}| > 1$ (6), error amplification is possible

(6) It can be shown that the value $|\mu_{\max}| \rightarrow 1$ as $x/h \rightarrow \infty$.

in all cases. It appears in the calculations (7) that the value of μ_{\max} was usually much larger than the next largest eigenvalue, so that in the most favorable case we can figure on an amplification factor of $\sqrt{\mu_{\max}/n}$ for the length of the error vector. But even then error amplifications are still possible, so that we get no statement about the stability from study of one step in the calculation.

Next, we consider the second part of (29), namely, $\varphi_m = R_m \varphi_0$ and investigate how the length of the error vector φ_0 has changed after a total of m steps. With exactly the same considerations as above, this leads to study of the eigenvalues $\omega_j = 0$ of the matrix $R'_m R_m$. The product matrix R_m also depends on the position x_0/h , for which the error φ_0 is assumed. The values of ω_{\max} were computed for a number of matrices $R'_m R_m$. The results for H-profiles of the similar solutions are shown in Figure 9. Because of computer memory limitations, only values up to $n = 20$ could be investigated.

The ω_{\max} curves always begin at the value $\mu_{\max}(x_0)$, first rising and then after some steps falling quickly below the value $\omega_{\max} = 1$. Then all the $\omega_j < 1$ and the error vector has certainly become smaller. As the value ω_{\max} also extends far beyond the next largest eigenvalue, then in the most favorable case we have the amplification factor $\sqrt{\omega_{\max}/n}$ for the error length. In the general case, then, the error has always become smaller before the value $\omega_{\max} < 1$ has been reached.

The explanation for the drop-off of the ω_{\max} curve lies in the spectrum of the μ_j . To be sure, there appears at least one value of $\mu_j > 1$, as well as other values of $\mu_j < 1$ which reduce the amplifications of the preceding steps, as the eigendirections of the various μ_j are different at every point. Now if we study the values of ω_{\max} for a general outer flow $U(x)$, in which $\lambda(x)$ and so the H-profile change with x , then

(7) Simultaneous iteration for two eigenvalues by the von Mises method.

the eigendirections of the μ_j change even more strongly and so produce smaller values of ω_{max} than for $|\lambda| = \text{constant}$. The ω_{max} curve was calculated for the flow around a cylinder (see Section 10c) at $n = 20$; it is plotted in Figure 9. This curve scarcely differs from the corresponding curve for $|\lambda| = 1$, although $\lambda \rightarrow \lambda_{\text{separation}}$ for the cylinder and the curves for $\lambda = 0$ or for $|\lambda|_{\text{separation}}$ lie above the curve for $|\lambda| = 1$.

It was possible to confirm the result of the stability study by numerical stability tests. Artificially introduced errors at arbitrary values of x/h and n were rapidly decreased. This was involuntarily confirmed by the fact that a calculation started accidentally with a separation profile gave the same separation point as one started with the stagnation point profile, within the limits of computing accuracy, for cylindrical flow.

6. EXPERIENCE WITH AN EXPLICIT METHOD AND A MULTIPOINT METHOD

Along with the implicit method described here, two other methods were studied. With the implicit method described in this work, the value H_x in (21) is calculated by Equation (15) taken at the point $(i + 1, k)$. In the explicit methods, H_x is formed from Equation (15) taken for the point (i, k) . In the multipoint method it is formed from an average of Equations (15) for i and $i + 1$. The last two methods were described extensively by Schönauer ⁽⁸⁾. Here we report only the information obtained there with respect to the stability of this method.

In the explicit method it appeared that we must have

$$4 \frac{n^2 h}{(2 - \lambda)x} \frac{H_{i,k}}{\xi} \leq 1$$

for stability. That means, for instance, that h must be

(8) See Footnote (1).

equal to or less than 10^{-4} for $|\lambda| = 1$, $n = 10$, $x = 0.1$. A larger value for h destroys the solution after a few steps. If the required computing accuracy would allow a step width of $h = 10^{-2}$, then a hundred times the computing cost would be needed for stability reasons. Therefore, this explicit method is not suitable for practical application.

/181

In the multipoint method, as in the implicit method, the eigenvalues μ_j of the matrices $S'_m S_m$ and the eigenvalues ω_j of $R'_m R_m$ are calculated. Such high values appear that destruction of the solution must be expected with a sufficiently large error. It is possible to calculate with this method as long as no large errors are allowed. But it is no longer possible to differentiate between method errors and amplified rounding errors, so that no reliable results are obtained.

7. CALCULATION OF THE SIMILAR H-PROFILE

For $x = \text{constant}$, $|\lambda| = \text{constant}$, so that the H-profile is also approximately constant, at least if it is almost similar to the H-profile of $|\lambda|$. Then the stability matrix S is also constant. In the program which is available anyway for calculation of the H-profile, one also suppresses the command to enumerate the x . In this way one always takes the solution profile for the x -interval again as the starting profile for the same interval.

According to (29), for $S = \text{constant}$, $g_m = S^m g_0$. If $\kappa_{\max} < 1$ for the maximum eigenvalue of S , then $S^m \rightarrow 0$ for $m \rightarrow \infty$ so that the initial error φ_0 vanishes. Thus we have an iteration method for computation of the similar solutions, because when $|\lambda| = \text{constant}$ the error φ_0 is the deviation of the initial profile from the similar solution.

Numerical calculation of a large number of eigenvalues showed that we always have $\kappa_{\max} \leq 1$ for the methods described here. The fastest convergence appears at point x/h , at which κ_{\max} has the minimum value. This is the case for $x_0/h = 0$ or

for $x_0/h = 1$. There, one can generate the similar H-profile after 5 to 30 steps, depending on the starting profile and the required accuracy. That is, we can use $H(\zeta) \equiv 1$.

TABLE 1
WALL VALUE OF THE SIMILAR H-PROFILE AT $\lambda = 1, \lambda = 0$ AND
VARYING MESH NUMBER n

n	$H_0(\lambda = 1)$	$H_0(\lambda = 0)$
∞	0,759636	0,110262
300	0,759733	0,110368
200	0,759805	0,110734
100	0,760051	0,111250
50	0,760659	0,112304
20	0,763107	0,115364
10	0,768554	0,119666
5	0,783003	0,124672

Table 1 shows the wall values $H_0 = \hat{H}(\zeta = 0)$ of the H-profile, Figure 5, for $\lambda = 1$ and $\lambda = 0$ with various values of n . The value for $n = \infty$ was calculated by Rauer ⁽⁹⁾. The H-profile and, with it, the wall values, depend on n , so that they give a view of the accuracy of the method. It is striking that the value of H_0 still shows an absolute error of 10^{-4} even for $n = 300$. For an absolute error of 10^{-3} we must have $n \approx 50$, and $n \approx 10$ is needed for an error of 10^{-2} . The dependence of the error on the value of n is investigated in the following section.

8. ERROR DEPENDENCE ON THE MESH WIDTH

a. Error in the ξ -direction.

Approximation errors due to a finite strip number, n , arise in the ξ -direction due to the central differences (19). We commit such an error in each Equation (15). In comparison,

(9) See reference [8].

we can neglect the errors of the wall equation (23). Then, instead of (27), we obtain the equation

$$CH_{i+1} = r + f, \quad (32)$$

in which f is the error vector which has the components:
 $f_0 = 0$, for $k = 1$ to $k = n - 1$

$$f_k = -\frac{1}{6n^2} \{ H H^{IV} - [2 H' + \lambda(1 - \xi^2)] H''' \}. \quad (33)$$

If the term in braces, $\{ \}$, in (33) were a constant independent of n , then the error vector would be proportional to $1/n^2$. A study of the H_0 values given in Table 1 for their dependence on n shows that the errors of the H_0 values are approximately proportional to n . This means that the term in braces, $\{ \}$, in (33) itself varies strongly with n , because of the fluctuation of the higher derivatives H''' and H^{IV} . It is sufficient that a large value of f_k appear at a point k . From the formal solution of (32): $H_{i+1} = C^{-1}r + C^{-1}f$ we see that this component is distributed over the entire solution H_{i+1} .

182

b. Error in the x-direction.

An approximation error in the x-direction arises through the difference quotients (21) and the linearization (24). We again obtain an erroneous equation (32) with $f_0 = 0$, and, for $k = 1$ to $k = n - 1$

$$f_k = h \left[2 H'' H_x - H' H_{xx} - \frac{A\xi}{2} H_{xx} \right]. \quad (34)$$

The error is proportional to the step width h if the term in brackets in (34) is constant. The bracketed expression can take on large values if H_x or H_{xx} are large. So as to calculate over-all with about the same approximation error, it is desirable to compute with smaller steps where H_x or H_{xx} are larger than in the rest of the range. The course of H depends on $U(x)$ and is easily determined by a coarse sample calculation.

It is convenient to choose the step width h so large that the approximation error in the x -direction for a single step is about one-tenth of the error which Table 1 shows for the n used. A higher expenditure for computing in the x -direction does not improve the accuracy because the attainable accuracy is limited by the value of n . Accumulation of single errors in the x -direction is not to be expected, according to the results from Section 5, as each error can be considered as a small perturbation φ_0 of the true profile, which is removed after a few steps.

9. COMMENTS ON PRACTICAL CALCULATION

It is practical to set up the program for solution of (27) so that the functions $U(x)$, $A(x)$ and $\lambda(x)$ are provided to the main program by a subprogram with the argument x . Calculation for various velocities $U(x)$ is done by exchange of this subprogram.

Now we shall state the relations by which the practically interesting quantities can be calculated from the H -profile. In order to obtain dimensionless quantities, we again use the reference length L introduced in Section 2b, along with a reference velocity U_∞ with which $U(x)$ is made dimensionless.

For the wall shearing stress τ_0 we obtain, using (3), (7), (9), (13), and (14):

$$\frac{\tau_0(x/L)}{\rho U_\infty^2} \sqrt{\frac{U_\infty L}{\nu}} = \sqrt{\frac{2 H_0}{A_L} \left(\frac{U}{U_\infty} \right)^3}, \quad (35)$$

where $H_0 = H(0, x/L)$. Analogously, we obtain the y -coordinate with (8):

$$\frac{y(x/L, \xi)}{L} \sqrt{\frac{U_\infty L}{\nu}} = \sqrt{A_L \frac{U_\infty}{U}} \int_0^\xi \frac{d\xi_1}{\sqrt{2 H(\xi_1, x/L)}}, \quad (36)$$

with ξ_1 as the integration variable. The integral is calculated in the examples of Section 10 by the right angle rule with the first derivative, with the points ξ_k of the difference

method as base points. The exact formulas for this can be found in Schönauer (10). The displacement thickness δ^* and the momentum loss thickness Θ are defined by

$$\delta^* = \int_{y=0}^{y=\infty} \left(1 - \frac{u}{U}\right) dy, \quad \Theta = \int_{y=0}^{y=\infty} \frac{u}{U} \left(1 - \frac{u}{U}\right) dy.$$

With $du/dy = u_y = t$ for a fixed position x , we obtain

$$\frac{\delta^*(x/L)}{L} \sqrt{\frac{U_\infty L}{\nu}} = \sqrt{A_L \frac{U_\infty}{U}} \int_{\zeta=0}^{\zeta=1} \frac{1-\zeta}{\sqrt{2H(\zeta, x/L)}} d\zeta, \quad (37)$$

$$\frac{\Theta(x, L)}{L} \sqrt{\frac{U_\infty L}{\nu}} = \sqrt{A_L \frac{U_\infty}{U}} \int_{\zeta=0}^{\zeta=1} \frac{\zeta(1-\zeta)}{\sqrt{2H(\zeta, x/L)}} d\zeta. \quad (38)$$

The integral is again computed by the right angle rule.

10. EXAMPLES

a. Preliminary comments

The examples were computed with the Zuse Z23 computer system at the Karlsruhe Technical College. A program was set up which computed with two different step widths h : with h_0 from x_0 to x_s ; and with h_1 for $x > x_s$. It was printed only at preset x -intervals, and only there were τ_w, δ^*, Θ and, if selected, also y_k computed. The strip number n has a double effect on the accuracy of y, δ^*, Θ : both the accuracy of the H -profile as well as the evaluation of the integrals by the right angle rule depend on the value of n through the n specified base points. The quantities y, δ^*, Θ are thus quite inaccurate for small n .

/183

(10) See Footnote (1), page 1.

b. Outside velocity, N1

The outside velocity N1, proposed by Nickel (11), is composed of a stagnation point flow with adjoining plane plate flow (Figure 10). It is

$$\left. \begin{aligned} 0 \leq \frac{x}{L} \leq 1: \frac{U}{U_\infty} &= \frac{x}{L}, \\ 1 < \frac{x}{L} < \infty: \frac{U}{U_\infty} &= 1. \end{aligned} \right\}$$

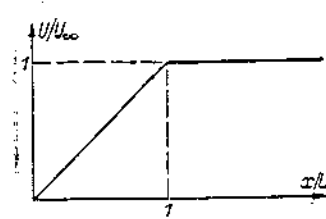


Figure 10. Outside velocity, N1

Figure 11 shows the results for $H_0, \tau_0, \delta^*, \theta$ for the calculation with $n = 100$, $h_0/L = 0.05$, $h_1/L = 0.1$, $x_s/L = 5$. The H-profile up to $x/L = 1$ is that of the stagnation point flow and is, therefore, independent of x and h constant. At the point $x/L = 1$, plane plate flow begins, and there U' has a jump. Thus, the "compatibility conditions" between the profile for $x/L = 1$ and the boundary conditions for $x/L > 1$ are not met, so that the solution H has a singularity at $x/L = 1$. This appears distinctly as the jump of the H_0 value in Figure 11.

As an accuracy comparison for different parameters n and h is not well representable analytically, numerical values for $H_0, \tau_0, \delta^*, \theta$ are given in Table 2. The table shows that an accuracy of two figures for τ_0 can be attained with relatively little computing cost, while high computing cost is required for an accuracy of three digits.

c. Cylinder with potential flow.

The boundary layer was calculated for the potential velocity of a cylinder with flow transverse to the axis. We have

(11) See reference [6].

$U/U_\infty = 2 \sin(x/R)$. Here R is the radius of the cylinder, which in this example is chosen as the reference length L . The quantity x/R is the angle in radians, measured from the stagnation point of the cylinder. The initial profile is the stagnation point profile (similar H-profile for $|\lambda| = 1$).

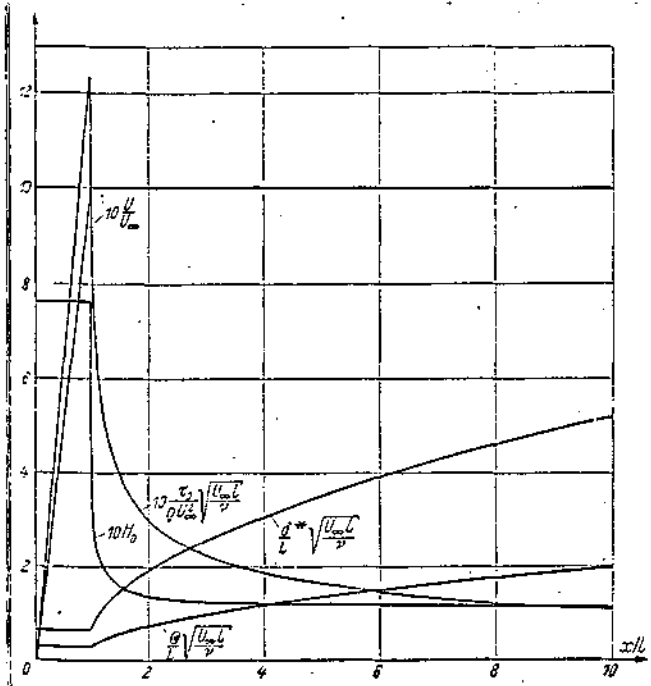


Figure 11. Outside velocity N1:
 $U, H_0, \tau_0, \delta^*, \theta$ for $n = 100$;
 $h_0/L = 0.05$; $h_1/L = 0.1$; $x_s/L = 5$.

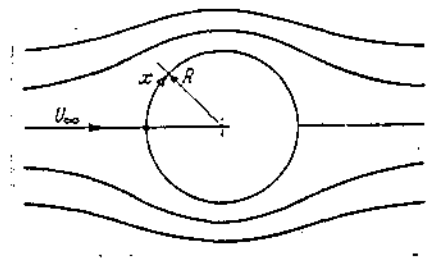


Figure 12. Flow around a cylinder

/185

Figure 13 shows the results for $H_0, \tau_0, \delta^*, \theta$ at $n = 100$, $h = 0.005$. At the separation point, $H_0 = 0$ and $\tau_0 = 0$. Goldstein [18], in a theory later improved by Stewartson [19], showed that in the vicinity of the separation point x_a the shear potential τ_0 varies as $(x_a - x)^{1/2}$. H_0 is proportional to τ_0^2 and so it varies as $x_a - x$ at the separation point. That is, the τ_0 curve opens at the separation point with a vertical tangent in the x -axis, and the H_0 curve like a linear function. The τ_0 and H_0 curves in the vicinity of the separation point are plotted in Figure 14 for different values of n and h . It should be noted that they are not expressed for each step of the computation.

TABLE 2. OUTSIDE VELOCITY N1: VALUES OF $H_0, \tau_0, \delta^*, \Theta$ (IN DIMENSIONLESS FORM) FOR DIFFERENT VALUES OF $n, h, \text{ AND } x/L$

/184

n	200	100	100	100	20	10	10
h	0.1	0.01	0.03	0.1	0.1	0.01	0.1
x/L	—	—	5	—	—	—	—
$x/L = 0.5$	$H_0 = 0.7593$	0.7600	—	—	0.7681	0.7683	—
	$\tau_0 = 0.6163$	0.6164			0.6177	0.6199	
	$\delta^* = 0.6466$	0.6454			0.6364	0.6262	
	$\Theta = 0.2911$	0.2901			0.2823	0.2742	
1	0.7593	0.7600	—	—	0.7631	0.7683	—
	1.2327	1.2329			1.2354	1.2398	
	0.6466	0.6454			0.6364	0.6262	
	0.2911	0.2901			0.2823	0.2742	
1.2		0.2012	0.2001	0.1993	0.2015	0.2064	0.2045
		0.5362	0.5346	0.5336	0.5365	0.5430	0.5405
		1.0848	1.0918	1.0965	1.0814	1.0473	1.0612
		0.4258	0.4297	0.4337	0.4215	0.4000	0.4081
1.5	0.1539	0.1568	0.1534	0.1541	0.1566	0.1633	0.1603
	0.3923	0.3959	0.3942	0.3926	0.3958	0.4041	0.4003
	1.4620	1.4482	1.4562	1.4646	1.4369	1.3870	1.4049
	0.5707	0.5603	0.5641	0.5681	0.5500	0.5221	0.5307
2	0.1342		0.1355	0.1345	0.1375		0.1415
	0.2991		0.3005	0.2994	0.3027		0.3072
	1.9133		1.8999	1.9080	1.8659		1.8192
	0.7392		0.7319	0.7355	0.7093		0.6829
4	0.1190		0.1199	0.1194	0.1231		0.1275
	0.1844		0.1850	0.1847	0.1875		0.1903
	3.0937		3.0766	3.0828	3.0019		2.9204
	1.1913		1.1817	1.1842	1.1372		1.0934
9	0.1139		0.1145	0.1143			
	0.1157		0.1161	0.1160			
	4.9260		4.9024	4.9066			
	1.8956		1.8819	1.8836			

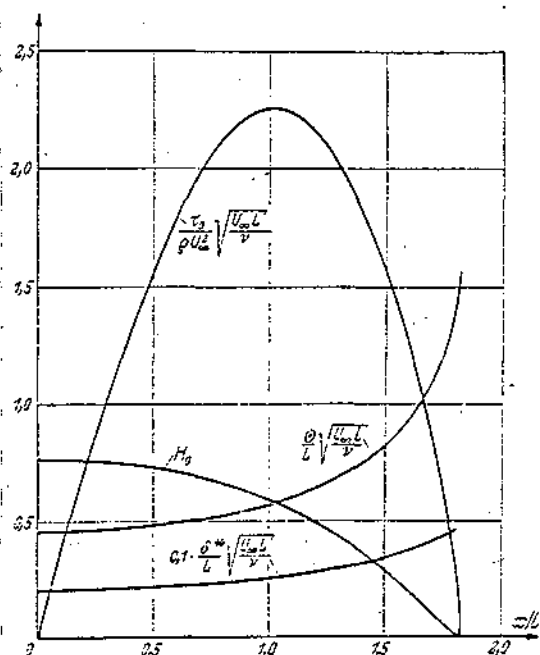


Figure 13. Flow around a cylinder: $H_0, \tau_0, \delta^*, \Theta$ for $n = 100, h/L = 0.005$.

TABLE 3. FLOW AROUND A CYLINDER: VALUES FOR $H_0, \tau_0/|H_0|, \delta^*, |\frac{\partial \phi}{\partial x}|$ IN DIMENSIONLESS FORM) WITH DIFFERENT VALUES OF n AND h

		Terrill	$n = 300$ $h = 0.005$	200	100	100	100	20	10	10
x_a/R		1.823	1.8234	0.905 1.823	0.505 1.822	0.41 1.819	0.1 1.803	0.01 1.817	0.01 1.808	0.1 1.796
0.3	$H_0 = -$	0.7457	0.7458	0.7460	0.7459	0.7438	0.7490	0.754	0.752	
	$\tau_0/ H_0 = 0.3569$	0.3569	0.3569	0.3569	0.3569	0.3564	0.3576	0.359	0.358	
	$\delta^* = 0.6595$	0.6587	0.6583	0.6570	0.6571	0.6586	0.6479	0.637	0.629	
	$ \frac{\partial \phi}{\partial x} = 0.2971$	0.2964	0.2960	0.2949	0.2949	0.2957	0.2873	0.279	0.279	
0.5	$-$	0.7201	0.7201	0.7204	0.7202	0.7163	0.7232	0.729	0.725	
	0.5575	0.5575	0.5575	0.5576	0.5574	0.5560	0.5587	0.561	0.559	
	0.6813	0.6805	0.6800	0.6787	0.6789	0.6817	0.6693	0.658	0.661	
	0.3061	0.3054	0.3050	0.3038	0.3039	0.3053	0.2959	0.287	0.288	
0.8	$-$	0.6526	0.6526	0.6529	0.6424	0.6453	0.6555	0.661	0.654	
	0.7550	0.7548	0.7549	0.7550	0.7548	0.7506	0.7565	0.760	0.756	
	0.7408	0.7400	0.7395	0.7381	0.7384	0.7442	0.7277	0.716	0.721	
	0.3303	0.3295	0.3291	0.3278	0.3280	0.3307	0.3192	0.310	0.312	
1.0	$-$	0.5833	0.5834	0.5837	0.5831	0.5730	0.5861	0.591	0.582	
	0.7979	0.7976	0.7977	0.7979	0.7974	0.7905	0.7995	0.803	0.796	
	0.8057	0.8051	0.8046	0.8030	0.8035	0.8129	0.7915	0.778	0.787	
	0.3560	0.3551	0.3546	0.3532	0.3535	0.3578	0.3438	0.333	0.337	
1.2	$-$	0.4888	0.4889	0.4892	0.4883	0.4747	0.4913	0.496	0.483	
	0.7611	0.7606	0.7607	0.7609	0.7602	0.7495	0.7625	0.766	0.756	
	0.9031	0.9027	0.9020	0.9001	0.9010	0.9168	0.8871	0.872	0.886	
	0.3927	0.3919	0.3913	0.3897	0.3901	0.3970	0.3792	0.368	0.374	
1.5	$-$	0.2850	0.2851	0.2853	0.2841	0.2643	0.2866	0.290	0.271	
	0.5520	0.5510	0.5511	0.5513	0.5502	0.5308	0.5526	0.556	0.537	
	1.1685	1.1689	1.1680	1.1654	1.1676	1.2071	1.1483	1.127	1.164	
	0.4826	0.4819	0.4812	0.4791	0.4799	0.4942	0.4656	0.451	0.464	
1.6	$-$	0.1982	0.1982	0.1984	0.1972	0.1764	0.1993	0.202	0.181	
	0.4396	0.4384	0.4385	0.4387	0.4373	0.4137	0.4397	0.442	0.419	
	1.3241	1.3252	1.3242	1.3212	1.3244	1.3821	1.3020	1.277	1.332	
	0.5281	0.5273	0.5265	0.5242	0.5252	0.5438	0.5092	0.492	0.510	
1.7	$-$	0.1043	0.1043	0.1045	0.1033	0.0841	0.1046	0.105	0.084	
	0.2989	0.2989	0.2989	0.2992	0.2975	0.2684	0.2993	0.300	0.269	
	1.5623	1.5611	1.5575	1.5624	1.5624	1.6535	1.5357	1.508	1.599	
	0.5854	0.5844	0.5818	0.5831	0.5869	0.6069	0.5650	0.546	0.569	
1.8	$-$	0.0149	0.0149	0.0149	0.0145	0.0021	0.0127	0.008		
	0.1049	0.1045	0.1045	0.1043	0.1030	0.0393	0.0965	0.077		
	2.0326	2.0349	2.0336	2.0299	2.0372	2.3011	2.0144	1.871		
	0.6628	0.6618	0.6608	0.6578	0.6592	0.6877	0.6394	0.623		

The separation point x_a was usually determined graphically as the zero point of the curve of the printed H_0 values. Later, a bisection process was built into the program. It begins at the first negative H_0 value and iteratively calculates the zero point of the H curve. In 1960, Terrill [20] first stated the separation point at $x_a/R = 1.823$, corresponding to $|\varphi| = 104.45$, after the separation point had previously been accepted as being at $|\varphi| \approx 109^\circ$. Terrill calculated the cylinder boundary layer with high numerical cost according to a difference-differential equation method. Table 3 shows Terrill's results and some results for different values of

n and h . As the calculations of Terrill and those of the author were done with $U = 1 \cdot \sin x$, the values for $\tau_0/\sqrt{2}, \delta^*/\sqrt{2}, \theta/\sqrt{2}$ are given in Table 3, if τ_0, δ^*, θ are the values for $U = 2 \sin x$. Table 3 shows again that, for example, we can calculate the shear stress with little cost to two decimals, but that the computing cost increases rapidly if three or four decimals accuracy are required. Some velocity profiles are plotted in Figure 15 for $n = 200, h = 0.01$.

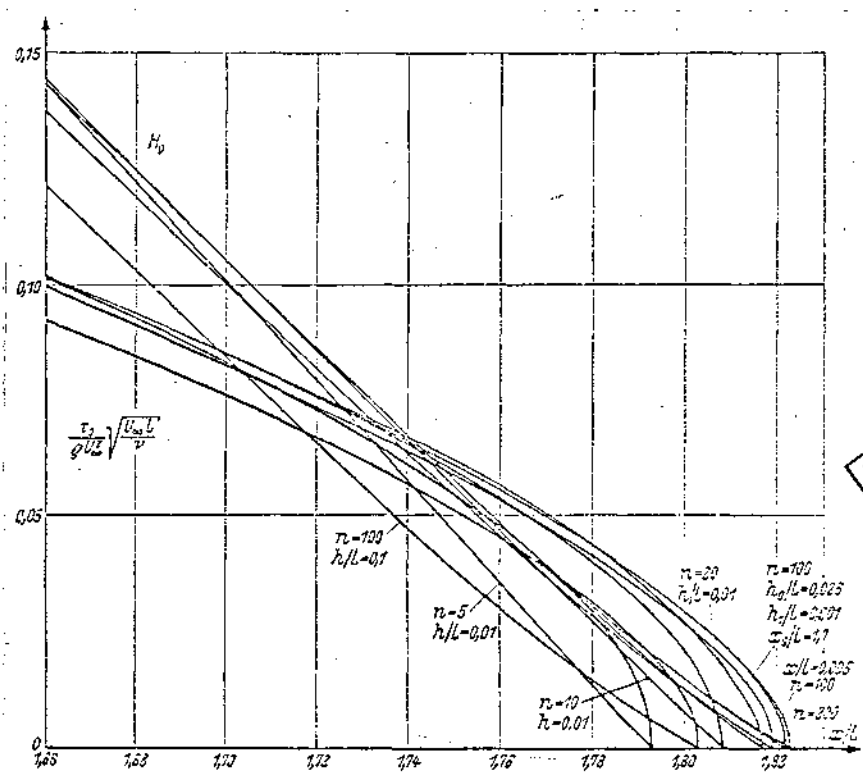


Figure 14. Flow around a cylinder: H_0, τ_0 in the vicinity of the separation point for different values of n and h/L .

d. Tani flow

The Tani flow, $U/U_\infty = 1 - (x/L)^m$ represents the potential flow at a flat plate in a diverging channel. The velocity curve is plotted in Figure 16 for different values of m . The initial profile \tilde{H} is the similar solution for $\lambda = 0$. For values of

$m > 1$ the velocity is $U/U_\infty \approx 1$ up to a certain point x_2/L , within the limits of computing accuracy, so that $\lambda \approx 0$ and one starts the boundary layer calculation only at the point $x_0 = x$ with the profile for $\lambda = 0$, as the H profile is constant up to there. First, H changes slightly, so that it can be computed with a coarse step width h_0 . Beyond a point x_s , where H_x or H_{xx} become larger, we calculate with a finer stepwidth h_1 . For values of $m < 1$ the velocity first falls rapidly, then more gradually. Here, we begin with a fine step width h_0 and beyond x_s we calculate with a coarser step width h_1 . In the range where $m \approx 1$ it is practical to compute with a constant h .

For $m = 1$, the Tani flow was treated with the series method of Howarth [21], with the differences-differential equation method of Hartree [22] and specially in the vicinity of the separation point by Leigh [23]. With the series method, Tani calculated the flow for $m = 2, 4, 8$ [24]. Görtler and Witting [25] calculated it for $m = 1, 2, 3, 4, 5$. As the series converge poorly in the vicinity of the separation point, the calculations were done there with different continuation methods.

187

The boundary layer was calculated with the differential method given here for 26 values of m between 0.05 and 100. For some values of m , control calculations were performed with different parameters n and h . In the limits of this work it is impossible to show the curves of $\tau_0, \delta^*, \theta, \eta_0$ for these examples. The results of Howarth (12), Hartree (13), and those of the differential method are given for some values of n and h .

(12) See reference [21].

(13) See reference [22].

TABLE 4. HOWARTH FLOW $U/U_\infty = 1 - x/L$: VALUES FOR $H_0, \tau_0, \delta^*, \Theta$ WITH DIFFERENT VALUES OF n AND h .

x/L	Howarth 0,12000	Hartree	$n = 300$ $h = 5 \cdot 10^{-4}$ 0,12033	200 $2,5 \cdot 10^{-4}$ 0,12019	200 $5 \cdot 10^{-4}$ 0,12027	100 10^{-4} 0,12065	100 $2 \cdot 10^{-4}$ 0,12072
x/L	$H_0 =$		0,0859	0,0862	0,0861	0,0865	
0,025	$\tau_0 = 1,772$	1,7772	1,7737	1,7761	1,7761	1,7789	
	$\delta^* = 0,292$		0,2909	0,2904	0,2905	0,2894	
	$\Theta = 0,110$		0,1091	0,1088	0,1088	0,1082	
0,050			0,0613	0,0615	0,0614	0,0610	0,0615
	1,011	1,0106	1,0120	1,0138	1,0133	1,0161	1,0140
	0,447		0,4458	0,4450	0,4451	0,4434	0,4440
	0,162		0,1616	0,1612	0,1612	0,1602	0,1603
0,075			0,0371	0,0372	0,0372	0,0375	
	0,613		0,6131	0,6146	0,6143	0,6171	
	0,603		0,6019	0,6007	0,6009	0,5983	
	0,209		0,2079	0,2073	0,2074	0,2060	
0,100			0,0145	0,0146	0,0146	0,0150	0,0150
	0,315	0,3154	0,3164	0,3175	0,3176	0,3213	0,3214
	0,794	0,7948	0,7925	0,7909	0,7910	0,7867	0,7870
	0,254	0,2542	0,2531	0,2524	0,2524	0,2507	0,2509
0,120			0,0002	0,0001	0,0002	0,0004	0,0004
	0,000		0,0302	0,0228	0,0316	0,0356	0,0473
	1,110		1,0708	1,0110	1,0559	1,0317	1,0335
	0,290		0,2902	0,2896	0,2895	0,2874	0,2874

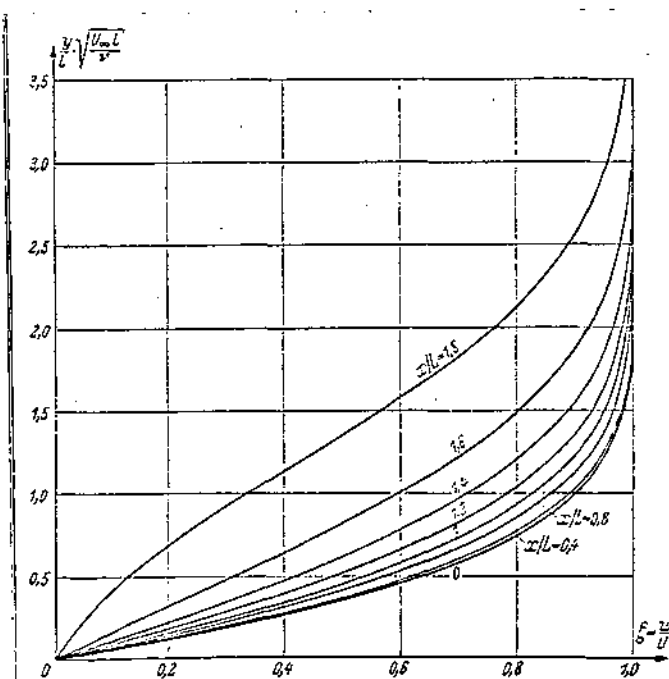


Figure 15. Flow around a cylinder; velocity profile for $n = 200$; $h/L = 0.01$.

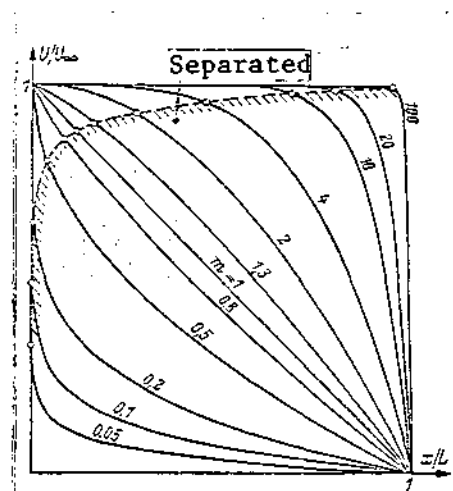


Figure 16. Outside velocity of the Tani flow for different values of m with the separation points.

TABLE 5. TANI FLOW: SEPARATION POINT x_a/L FOR $U/U_\infty = 1 - (x/L)^m$

/188

m	x_a/L	n	h_0	h_1	x_g/L
0,05	$3,24 \cdot 10^{-1}$	100	$2 \cdot 10^{-8}$	$2,5 \cdot 10^{-8}$	$2,5 \cdot 10^{-6}$
0,05	$3,29 \cdot 10^{-1}$	100	$2 \cdot 10^{-7}$	$5 \cdot 10^{-6}$	$2 \cdot 10^{-5}$
0,1	$1,184 \cdot 10^{-3}$	100	$5 \cdot 10^{-7}$	10^{-5}	10^{-4}
0,1	$1,20 \cdot 10^{-3}$	100	10^{-6}	$2 \cdot 10^{-5}$	10^{-4}
0,2	$5,465 \cdot 10^{-3}$	100	$2 \cdot 10^{-6}$	$5 \cdot 10^{-5}$	$5 \cdot 10^{-3}$
0,2	$5,462 \cdot 10^{-3}$	100	10^{-5}	10^{-4}	$6 \cdot 10^{-3}$
0,3	0,01343	100	10^{-5}	10^{-4}	10^{-3}
0,3	0,0136	100	$2 \cdot 10^{-5}$	$2,5 \cdot 10^{-4}$	10^{-3}
0,5	0,0382	100	10^{-4}	$2,5 \cdot 10^{-4}$	0,01
0,8	0,0864	100	$2,5 \cdot 10^{-4}$	$5 \cdot 10^{-4}$	0,02
1	0,12033	300	$5 \cdot 10^{-4}$	$5 \cdot 10^{-4}$	—
1	0,12019	200	$2,5 \cdot 10^{-4}$	$2,5 \cdot 10^{-4}$	—
1	0,12037	200	$5 \cdot 10^{-4}$	$5 \cdot 10^{-4}$	—
1	0,12065	100	0,001	0,001	—
1	0,12072	100	0,002	0,002	—
1,3	0,1705	100	0,001	0,001	—
1,6	0,2165	100	0,001	0,001	—
2	0,2724	100	0,0025	0,0025	—
3	0,3825	100	0,0025	0,0025	—
4	0,4624	100	0,001	0,001	—
4	0,4629	100	0,0025	0,0025	—
4	0,4622	50	0,001	0,001	—
5	0,5231	100	0,01	0,0025	0,2
6	0,5712	100	0,01	0,0025	0,25
7	0,6091	100	0,01	0,0025	0,28
8	0,641	100	0,01	0,0025	0,32
10	0,6901	100	0,01	0,0025	0,39
12	0,7265	100	0,01	0,0025	0,45
16	0,7771	100	0,01	0,0025	0,46
16	0,7765	50	0,0025	0,001	0,46
16	0,7739	20	0,005	0,005	—
20	0,8112	100	0,01	0,0025	0,55
20	0,8107	50	0,0025	0,001	0,55
20	0,7985	20	0,005	0,005	—
25	0,8408	100	0,01	0,0025	0,6
25	0,8401	50	0,0025	0,001	0,6
25	0,8401	50	0,01	0,004	0,6
30	0,8615	100	0,01	0,0025	0,65
40	0,8905	100	0,01	0,001	0,73
40	0,8902	100	0,0025	0,0025	—
40	0,8885	20	0,0025	0,0005	0,85
50	0,9078	200	0,0025	0,0005	0,78
50	0,9076	100	0,0025	0,0005	0,78
50	0,9070	100	0,01	0,005	0,78
50	0,9067	100	0,02	0,01	0,78
50	0,9065	20	0,0025	0,0005	0,85
50	0,9065	20	0,0025	0,0025	—
50	0,9048	10	0,0025	0,0005	0,85
75	0,9344	100	0,01	0,001	0,83
100	0,94956	100	0,005	0,0005	0,87
100	0,9492	100	0,01	0,001	0,85
100	0,9495	100	0,005	0,005	—
100	0,949	100	0,01	0,01	—

For the flows with $m \neq 1$, only the separation points x_a will be stated as characteristic quantities. As for the cylinder, they were determined either graphically or with the bisection procedure from the H_0 curve. The results with the check calculations are shown in Table 5. The accuracy of the separation point could be about 3 figures for the calculation parameters used. In Figure 17, the separation points from Table 5 are plotted vs. $\log m$ in the form $\log \frac{x_a/L}{1-x_a/L}$

so as to represent all the points with about the same accuracy.

The separation points are plotted in Figure 16. The velocity at which the boundary layer separates is plotted vs. $\log m$ in Figure 18. At large values of m , the boundary layer thickness grows with almost constant outside velocity, and the boundary layer flow loses energy. Now, if we insert a somewhat stronger drop in velocity (pressure increase), the boundary layer separates immediately, and at $m = 100$, almost with full velocity U_∞ , Figure 18. With very low values of m there is a sudden drop in velocity at the point $x = 0$; but here the boundary layer thickness is zero and the boundary layer is compatible with a considerably higher velocity drop than at $m > 1$. At $m = 0.05$ it is up to some 35% of U_∞ . Whether such flow is realizable, and whether the boundary layer assumptions still apply here ⁽¹⁴⁾ will not be investigated. The results given here are properties of the mathematical models (1), (2), the solution of which by the differential method can be considered reliable even for such extreme cases as $m = 100$ or $m = 0.05$.

/189

(14) See references [1] and [2].

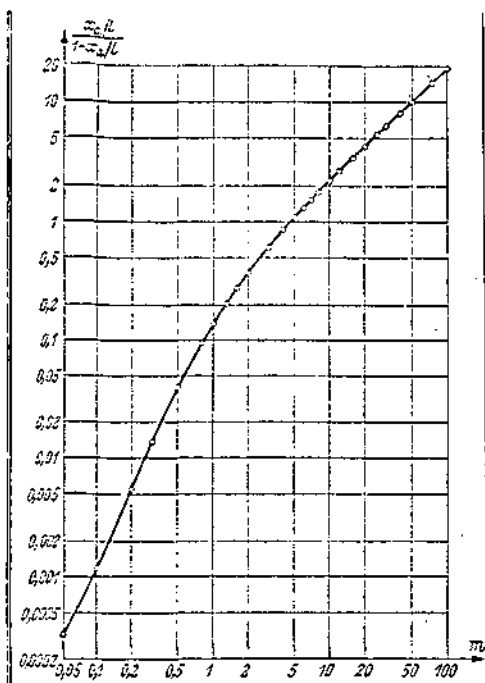


Figure 17. Tani flow: $(x_s/L)/1 \rightarrow (x_s/L)$ with x_s as the abscissa of the separation point, as a function of m .

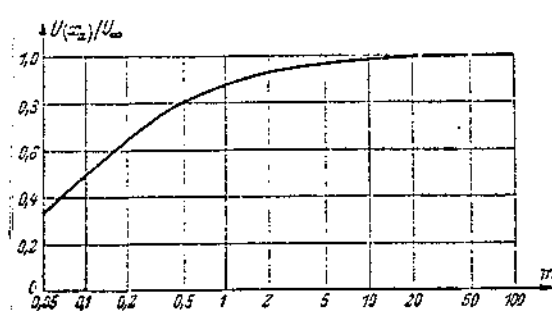


Figure 18. Tani flow: outside velocity at the separation point as a function of m .

11. SUMMARY

An implicit differential method is given for the laminar incompressible steady boundary layer at a solid impermeable wall. It uses a differential equation of the Crocco type as the starting equation. By detailed stability investigations which can only be done numerically, it can be shown that perturbations are definitely removed after a few steps of calculation. The method is tested practically with a large number of examples. The computing time requires the use of electronic computers, but the method is well suited for programming. For example, an accuracy of two decimals for the shear stress is attained with little cost, while the cost for an accuracy of three decimals must be considered as relatively high.

I thank Prof. Dr. K. Nickel, who stimulated this work, for the valuable advice which he has supplied for it. I also thank Dr. R. Krawczyk for fruitful discussions about stability, and for many suggestions on this problem.

(Received 11 June 1963)

Author's address: Dr. Willi Schönauer, Karlsruhe,
Englerstrasse 7, Institut für Angewandte
Mathematik der Technischen Hochschule.

REFERENCES

1. Schlichting, H. Boundary Layer Theory. Abschnitt III, Karlsruhe, 1958.
2. van Dyke, M. J. Fluid. Mech., Vol. 14, 1962, p. 161.
3. Falkner, V. M. and S. W. Skan. Phil. Mag., Vol. 12, 1931, p. 865; ARC Rep. 1314, 1930.
4. Hartree, D. R. Proc. Roy. Soc., London, Vol. A 161, 1937, p. 353.
5. Crocco, L. Monografie scientifiche di aeronautica, No. 3, Rom, 1946.
6. Nickel, K. and T. H. Karlsruhe. Verbal communication at a boundary layer seminar, 1961.
7. Gadd, G. E. ARC Techn. Rep. CP 312, London, 1957.
8. Rauer, H. J. and T. H. Karlsruhe. Verbal communication.
9. Schröder, K. FB 1741, 1943, Math. Nachr, Vol. 4, 1951, p. 439.
10. Görtler, H. Ing.-Arch., Vol. 16, 1948, p. 173.

11. Witting, H. Z. Angew. Math. Phys., Vol. 4, 1953, p. 376.
12. Rheinboldt, W. J. Rat. Mech. a. Analysis, Vol. 5, 1956, p. 539.
13. Siekmann, J. Dissertation T. H. Karlsruhe, 1955.
14. Flügge-Lotz, I. Fifty Years of Boundary Layer Research, p. 393, Braunschweig, 1955.
15. Kramer, R. F. and H. M. Lieberstein. J. Aero/Space Sciences, Vol. 26, 1959, p. 508.
16. Fiebig, M. Z. angew. Math. Mech., Special issue of the GAMM-meeting, 1962.
17. Krawczyk, R. and T. H. Karlsruhe. Publication in process.
18. Goldstein, S. Quart. J. Mech. a. Appl. Mathem., Vol. 1, 1948, p. 43.
19. Stewartson, K. Quart. J. Mech. a. Appl. Mathem., Vol. 11, 1958, p. 399.
20. Terrill, R. M. Phil. Transact. Roy. Soc., London, Vol. A 253, 1960, p. 55.
21. Howarth, L. Proc. Roy. Soc., London, Vol. A 919, No. 164, 1938, p. 547.
22. Hartree, D. R. ARC Rep. a. Mem., 1949, p. 2426.
23. Leigh, D. C. F. Proc. Cambr. Phil. Soc., Vol. 51, 1955, p. 320.
24. Tani, I. J. Phys. Soc., Japan, Vol. 4, 1949, p. 149.
25. Görtler, H. and Witting, H. Österr. Ing.-Arch, Vol. 11, 1957, p. 111.

Translated for National Aeronautics and Space Administration under contract No. NASw 2035, by SCITRAN, P.O. Box 5456, Santa Barbara, California, 93108